Aalborg Universitet

AALBORG UNIVERSITY
DENMARK

Mutual Coupling Suppression with Decoupling Ground for Massive MIMO Antenna Arrays

Zhang, Shuai; Chen, Xiaoming; Pedersen, Gert Frølund

Mutual Coupling Suppression with Decoupling Ground for Massive MIMO Antenna Arrays

Shuai Zhang, *Senior Member, IEEE*, Xiaoming Chen, *Senior Member, IEEE*, and Gert Frølund Pedersen, *Senior Member, IEEE*

Abstract— A concept of decoupling ground (DG) is introduced in this paper to enhance the isolation of massive MIMO antenna arrays. For an array, mutual coupling between array elements can be achieved by the free-space coupling and the coupling currents flowing on the ground plane shared by elements. The isolation in this paper is improved by adjusting the shape of the ground plane under each element to make the mutual coupling from the free space and the ground plane out of phase. In this way, low mutual coupling is realized. As the first example, a single-polarization linear array with 8 elements is designed, simulated and measured to verify the concept as well as the simulation accuracy. The measurements align very well with the simulations. Another two examples of dual-polarization 2×2 and 4×4 square arrays are also given and simulated to demonstrate the effectiveness of the proposed technique. In all of these examples, the isolation can efficiently be enhanced with the DG for all the co-polarization and cross- polarization coupling paths of the massive MIMO elements. Compared with the previous literature, the arrays with the DG method can achieve either much better isolation or a much lower profile while keeping the other performance comparable.

Index Terms— Isolation, decoupling, massive MIMO, antenna array.

I. INTRODUCTION

THE Multiple-input and multiple-output (MIMO) technologies are able to increase channel capacity without additional spectrum [1], [2]. As one of the key technologies for 5G cellular networks, massive MIMO is the extension of the conventional MIMO. A massive MIMO array utilizes a very large number of MIMO elements to significantly enlarge channel capacity and exploits the array directivity to effectively reduce interference [3]-[6]. The performance of massive MIMO systems highly depends on the isolation between array elements. From the MIMO capacity and symbol error rate point of view, mutual coupling below -17 dB and -15 dB is sufficient, respectively [7]. However, 15-17 dB isolation is not a satisfactory level for some other system factors, such as: active voltage standing wave ratio (VSWR), out-of-band (OOB)

emission suppression, and so on. During the transmission, random phases and amplitudes of signals will be excited at the ports of massive MIMO elements. The active VSWR can be up to 6 with 15 dB isolation [8], and the worst active VSWR can be much improved if the isolation is enhanced to over 25 dB [20]. The mutual coupling will also distort the linearity of the power amplifiers (PAs) behind each massive MIMO element, causing interferences to the adjacent-channel systems [9] (OOB emission issue). Typically, in industry, the inter-element isolation of massive MIMO arrays is much preferred to be over 25 dB or even higher. Since a large number of array elements have to be placed in a device (e.g., base stations) with the limited space, it is difficult to reduce the coupling by increase the inter-element distance. Furthermore, massive MIMO arrays of base stations typically require elements with dual polarization. The applied decoupling techniques should be able to reduce all the co-polarization and cross-polarization mutual coupling between all the adjunct, diagonal and other array elements simultaneously, which is a very challenging issue.

Different researches have been done on the isolation enhancement of MIMO arrays during the past few years [10]-[20]. For MIMO arrays with 2 or 4 elements, many decoupling techniques can be found such as: defected ground structures [10], parasitic scatterers [11], wideband neutralization line [12], beamforming network [13], metamaterials [14], reactively loaded dummy elements [15], characteristic modes [16], and so on. These methods can effectively reduce the mutual coupling but are very difficult to use for the array with many elements and dual polarization at the same time. In [17], a 20-port MIMO array with single polarization has been reported with ring-shaped decoupling elements. The array is extremely compact. However, the inter-element coupling is only lower than -10 dB with the total efficiency of about 30%. The massive MIMO array with dual-polarization cavity-backed dipoles has been proposed in [18], where the inter-element distance is 0.6 λ. However, the isolation is only better than 13 dB. A 144-port dual-polarized massive MIMO array has been introduced in [19], where several stacked patches with high gain are designed. The isolation is over 35 dB within the operating bands, but the whole array with a 3D structure is very bulky. A metamaterial-based planar lens has been utilized to design a massive MIMO array [20]. By switching between different ports, the directional beam can point in different directions. The inter-element isolation is high, but a very large lens-antenna

Shuai Zhang, and Gert Frølund Pedersen are with the Antennas, Propagation and Radio Networking section at the Department of Electronic Systems, Aalborg University, Denmark (email: sz@es.aau.dk).

Xiaoming Chen is with School of Electronic and Information Engineering, Xi'an Jiaotong University, Xi'an 710049, China (email: xiaoming.chen@mail.xjtu.edu.cn).

distance is required in this method. In [21], a concept of array-antenna decoupling surface (ADS) has been proposed for massive MIMO antennas. Reflections are constructed by small metal patches on the ADS to cancel the coupling. The simulated isolation is over 20 dB for a dual-polarization 2×2 array. However, the ADS is normally placed about λ/4 away from array elements in order to efficiently enhance isolation without distorting antenna radiation patterns. Low profile base station antennas are highly desirable in the industry for aesthetic reasons, yet the height of the array [21] is difficult to decrease.

In this paper, a concept of decoupling ground (DG) will be introduced. For an array (not printed on a substrate), the mutual coupling can be realized by the free-space coupling and the coupling currents flowing on the element-shared ground plane. Here, the mutual coupling is reduced by changing the shape of the ground plane under each element, so that the coupling from the free space and the ground plane can be out of phase and canceled with each other. A single-polarization linear array with 8 elements will be simulated and measured to verify the concept and the simulation accuracy. Another two examples of dual-polarization 2×2 and 4×4 arrays will also be simulated. In all of these cases, the isolation is enhanced efficiently. The novelties of this work are listed as follows:

1. Introduce a new decoupling method for a massive MIMO antenna array, which has not been reported previously.
2. The mechanism of the proposed method is analyzed and verified. It does not depend on the array operating frequency.
3. The proposed DG technique can be applied for the decoupling of an array with dual polarization and a large number of array elements.
4. The array with the DG method can realize either much better isolation or much lower profile (with the other performance comparable) than the previous literature.
5. Most of the previous work about small ground planes are to cut the coupling currents on the shared ground plane to reduce coupling, e.g. in [22]-[24], but the free space coupling is still available. This method uses the coupling current to cancel the free space coupling, so it is more efficient than the previous work in massive MIMO arrays.
6. In order to cut the coupling current in the previous work, the small ground planes are normally not shorted/grounded to the shared ground plane. It makes the element feeding and implementation more complicated. In our design, the small ground can be either connected or not connected to the shared ground plane, which is more flexible.

II. PROPOSED DECOUPLING TECHNIQUE

A. Diagram of the Proposed Decoupling Method

In this section, the operating principle of the proposed decoupling method will be explained. The parameters affecting the decoupling performance will be mentioned as well.
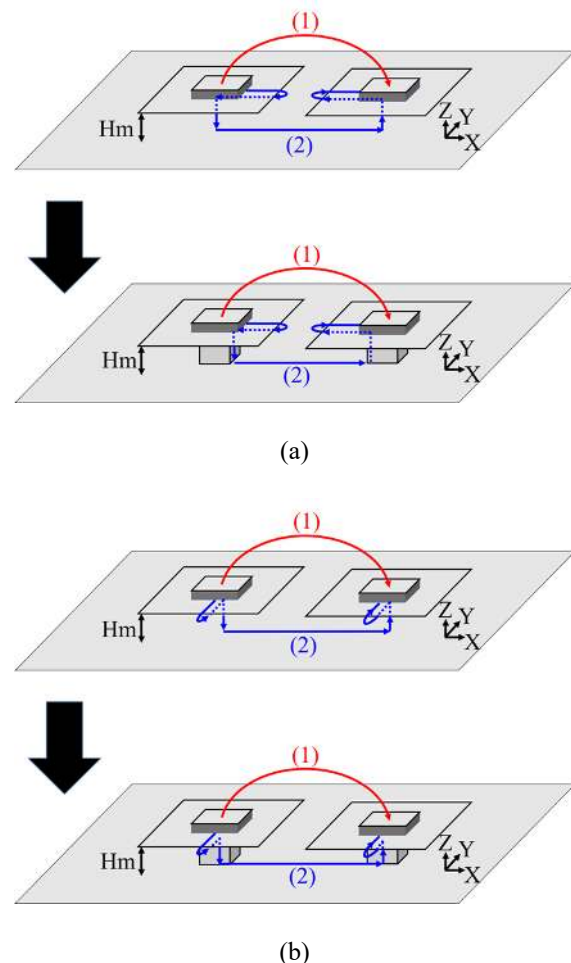

Fig. 1. Sketches of the decoupling ground concept for the MIMO elements. Free-space coupling (1) and current coupling (2) are out of phase in order to improve the isolation. (a) x-axis polarized MIMO elements: the coupling currents between the small and the shared ground planes can be formed by displacement currents (the upper subfigure) or by surface currents on metal cylinders (the below subfigure). (b) y-axis polarized MIMO elements: the coupling currents between the small and the shared ground planes can be formed by displacement currents (the upper subfigure) or by surface currents on metal cylinders (the below subfigure).

Fig. 1 (a) shows the sketch of the decoupling ground concept for MIMO elements with x-axis polarization. Two patch antennas with their own small ground planes are placed above a shared big ground plane with the distance of Hm. The mutual coupling can be achieved in two ways: free-space coupling (1) and current coupling (2) (see Fig. 1 (a)). Please note that the coupling currents between the small ground plane and the shared ground plane can be formed by displacement currents. By properly adjusting the small ground plane sizes in the x-axis direction and the Hm, the coupling path (1) and (2) can be out of phase and canceled with each other. Metal cylinders are added between the small ground plane and the shared ground plane, so the antennas can be easily fed by coaxial cables running through the inside of the cylinders. Apparently, the coupling currents between the small ground plane and the shared ground plane are connected by the external surface of the metal cylinder. And the width of the cylinder in the x-axis direction will affect the length of the coupling current

path (2). In the following, we define the small ground plane and the metal cylinder as the decoupling ground (DG). The DG concept for the MIMO elements with y-axis polarization is illustrated in Fig. 1 (b). The principle here is similar to that with x-axis polarization, so will not be explained again.

The decoupling performance mainly depends on the configuration of the DG. If MIMO elements are x-axis polarized (see Fig. 1), the decoupling performance (and also the coupling path (2)) is determined by the height of Hm, the width of the small ground plane and the metal cylinder in the x-axis direction. If MIMO elements are y-axis polarized (see Fig. 1), it is determined by the height of Hm, the width of the small ground plane and the metal cylinder in the y-axis direction.

B. Simulations for the Verification of the Proposed Decoupling Method
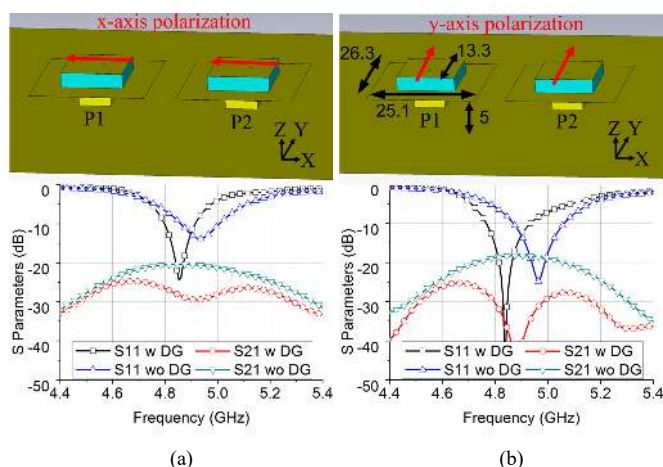

Fig. 2. (a) The configuration of x-axis polarized MIMO elements with DG (the upper subfigure), and the comparison of S parameters with/without DG (the below subfigure). (b) The configuration of y-axis polarized MIMO elements with DG (the upper subfigure), and the comparison of S parameters with/without DG (the below subfigure).

In order to verify the proposed DG method illustrated in Fig. 1, some simulations will be performed in this subsection.

Dual-element MIMO arrays with DG in x-axis polarization and y-axis polarization are shown in Fig. 2 (a) and (b), respectively. The arrays with the x-axis and y-axis polarization have the same configurations, but with different feeding positions in order to excite different polarizations. In the arrays, each element is a square patch antenna printed on a dielectric block of Epsilam 6 with a permittivity of 6 and a loss tangent of 0.002. Higher dielectric permittivity can make the patch antenna smaller, which will lower the mutual coupling between the elements as well. The thickness of the substrate is 3.18 mm. The detailed array geometry is also given in Fig. 2. The S parameters of the arrays with and without DG for the x-axis and y-axis polarization are provided in Fig. 2 (a) and (b), respectively. The port-to-port isolation can clearly be improved by over 10 dB with the proposed decoupling method. The impedance matching of the arrays with DG is tuned slightly to the lower frequencies within the band of 4.8-5 GHz. This is for the purpose that: during all the studies in the next paragraph, we will keep the antenna array geometry (in Fig. 2) the same and also make sure the impedance matching of the antenna always

better than -6 dB within 4.8-5 GHz.

Fig. 3 illustrates the analyzing procedures in order to verify the proposed decoupling method (illustrated in Fig. 1). In Step A, an absorber, made of C-RAM MT 26, is added under the small ground plane. According to the datasheet of C-RAM MT 26, the relative permittivity and the loss tangent of the absorber are around 2.8 and 3.31 in the target band of 4.8-5 GHz, respectively. In this way, only free-space coupling (1) (see Fig. 1) between two antenna elements are available. This is labeled as Case 1. In Step B, we further add one more absorber between two antennas. The added absorber should be as large as possible but without touching the small ground plane as well as affecting the antenna performance. In this scenario, both the coupling path (1) and (2) in Fig. 1 should not be suppressed. In the simulations, the S21 of two antennas is lower than -30 dB, which can be treated as no mutual coupling. In Step C, we remove the absorber under the small ground plane, while keeping the absorber between two antennas. This case is labeled as Case 2, where two antenna elements are only coupled through the current coupling (2) (see Fig. 1), which is affected by DG configurations.
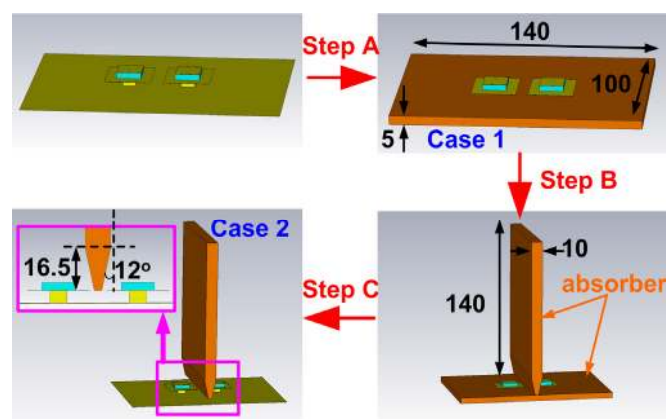

Fig. 3. Simulation processors for the verification of the proposed decoupling method: In Step A, an absorber is added under the small ground planes of elements in order to eliminate the current coupling path (2). In Step B, one more absorber is placed between two antennas in order to eliminate both the free-space coupling path (1) and the current coupling path (2). In Step C, the absorber under the small ground plane is removed, while keeping the absorber between two antennas, where only the free-space coupling path (1) is available.

If the DG decoupling method is correct, the complex S21 of the two antenna ports in Case 1 and Case 2 should be out of phase and canceled. Fig. 4 (a) shows the phase difference, real and imaginary part of S21 in Case 1 and Case 2 for the array with x-axis polarization. It can clearly be observed that the S21 in the two cases are nearly 180-degree phase difference. Furthermore, the real and imaginary parts of S21 in Case 1 and Case 2 are also given in Fig. 4 (a) and are canceled. The similar phenomena are also observed for the array with y-axis polarization in Fig. 4 (b). Please note that the real and imaginary parts of the S parameters are used in Fig. 4 instead of the magnitude, because the real and imaginary parts give more information. The positive or negative of the real and imaginary parts indicate the phase information. These studies can verify

that there are two coupling ways which can be canceled with each other if the DG geometry is properly selected. It should be noticed that: (1) Here we use S21 instead of the mutual impedance of Z21 for studies. The reason is S21 takes all the impact of Z11, Z22, and Z21 into account. Once Z21 changes, Z11 and Z22 will also be a little different. It is better to study the cancelation of two coupling ways with S21 instead of Z21. (2) In Fig. 4, the real part of S21 is sometimes negative. This is not unphysical. For the voltage and current involved are at different locations, Z21 is possible to be negative. S21 is calculated with Z21, so it can also be negative.
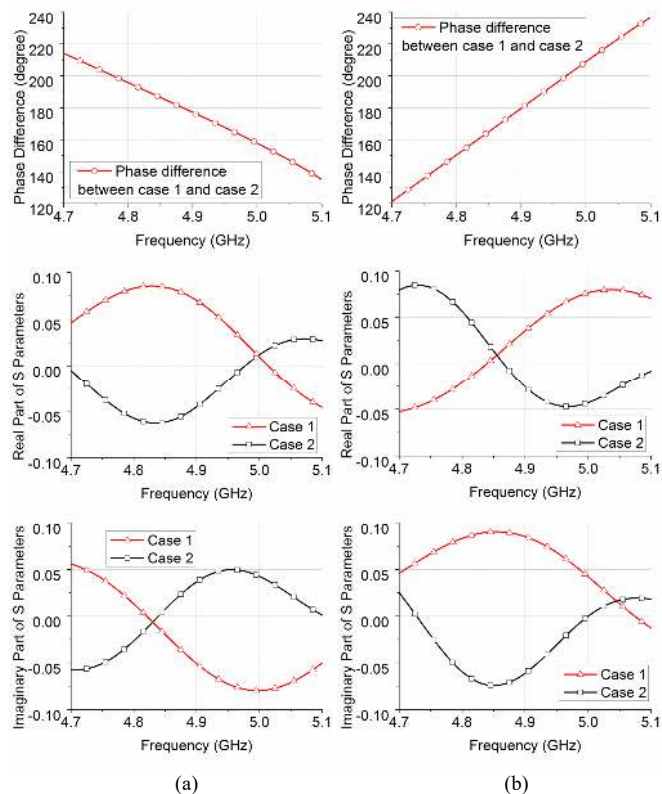

Fig. 4. Phase difference, real and imaginary part of S21 in Case 1 and Case 2 for: (a) the array with x-axis polarization, and (b) the array with y-axis polarization.

In order to better understand the mechanism, the current distributions of the array with x-axis polarization and y-axis polarization are shown in Fig. 5 (a) and (b), respectively. In general, the directions of the current flowing on the ground plane are very similar to the path (2) illustrated in Fig. 1. For example, the currents in Fig. 5 (a) flow from the x-axis direction of the small ground plane, via the x-axis-orientated metal cylinder surface, and then to the x-axis direction of the shared ground plane. It is the same as the predicted path (2) in the below subfigure of Fig.1 (a). Similarly, the currents in Fig. 5 (b) flow from the small ground plane, via the metal cylinder surface, and then to the shared ground plane, all in the y-axis direction, which is the same to the expected in Fig.1 (b). The current distributions in Fig. 5 further prove the correctness of the models in Fig. 1.

In the following, some design examples with the DG

technique will be provided for the isolation enhancement of a single-polarized linear array and dual-polarized square arrays.
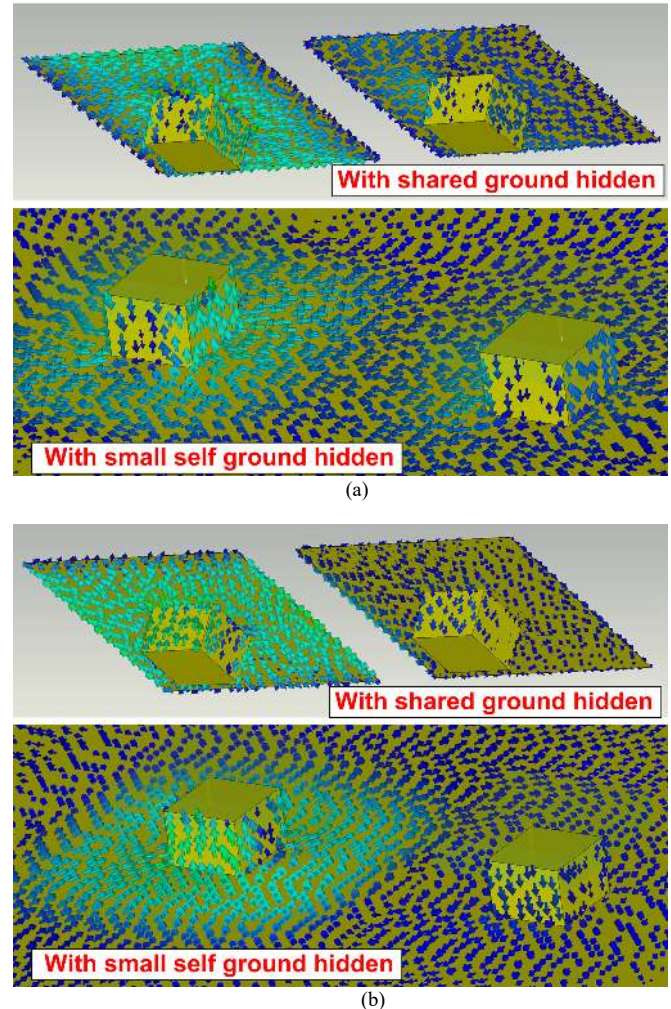

Fig. 5 (a) Current distributions of the x-axis polarized MIMO array (with the shared ground hidden or the small ground hidden), where the current-flowing directions are very similar to the predicted in the below subfigure of Fig.1 (a). (b) Current distributions of the y-axis polarized MIMO array (with the shared ground hidden or the small ground hidden), where the current-flowing directions are very similar to the predicted in the below subfigure of Fig.1 (b).

III. SINGLE-POLARIZATION LINEAR ARRAY

A. Antenna Configurations

The concept of the DG has first been applied to enhance the isolation for a single-polarization linear array. The configurations of the proposed array are shown in Fig. 6 (a). The antenna is proposed for the massive MIMO band of 4.8-5 GHz. The array consists of 8 elements with the inter-element distance d of 32 mm (0.52 λ_C). Each patch element is printed on the dielectric block of Epsilam 6 as well. The patch elements are placed on the DG structures that include small ground planes and metal rectangular cylinders. The edges of each small ground are not necessarily to be folded up as a cavity. But in this design, the folded-up edges can help slightly enlarge the edge-to-edge distance between the small ground planes of the neighboring elements (while keeping the path length of the

coupling current the same). This makes the amplitude of the free space coupling slight smaller. In general, with the inter-antenna distance around half wavelength or larger, the free space coupling is slightly larger than the current coupling, which can be observed from Fig. 4. With the folded-up edges, the two coupling paths have more similar amplitudes and opposite phases, so that the decoupling coupling is slightly better. The folded-up edges will not change the operating principle of the DG method. Each patch is fed by a coaxial cable with an SMA connector at the end. From the feeding position, it is easy to know that the mutual coupling between the neighboring elements occurs in the H plane of the patches. Two shorting pins are also added for each patch antenna in order to assemble the patch, the small ground, the metal cylinder, and the shared ground plane together. Please note that the short pins utilized here are mainly used to facilitate the antenna manual fabrication. Since the electric field of the shorting pin location is zero, the shorting pin will not affect the antenna and mutual coupling reduction performances. In practical applications, the small ground and the metal cylinder can be made into one piece, and then soldered to the shared ground plane. The shorting pins and the feeding cables are placed inside the metal cylinder (as shown in Fig.6 (a)) so that the antenna performance will not be influenced. The detailed antenna dimensions are listed in Table I. It should be noticed that the total array height (including DG) in this design is 0.14 λ_C, which is much lower than the linear array height of 0.31 λ_C with ADS in [21].

In order to verify the proposed DG concept and simulation accuracy, a prototype has been fabricated and shown in Fig. 6 (b). The compactness of the array can clearly be observed. The prototype has also been measured, and the measured results will be provided and discussed in the next subsection.

TABLE I
DETAILED DIMENSIONS OF THE DESIGNED ANTENNA ARRAYS (UNIT: MM)

Parameters	Wg	Lg	Hg	Lm	Hm	Lp	Wp
SLA	26.5	25	3.5	10.5	5	13.85	13.85
2×2 DSA	26.3	26.3	0	5	7	13	13
4×4 DSA	24.2	24.2	0	2	9	12.7	12.7
Parameters	Hp	df	df1	df2	Ri	Ro	Ang
SLA	3.18	4.53	N.A.	N.A.	N.A.	N.A.	0º
2×2 DSA	6	N.A.	3.5	3.5	1.8	3	16º
4×4 DSA	6	N.A.	3.35	3.35	1.2	3	18º

SLA, 2×2 DSA, and 4×4 DSA are the abbreviations of single polarization array, dual-polarization 2×2 square array, and dual-polarization 4×4 square array, respectively.

B. Array Performance

Fig. 7. The simulated and measured S parameters of the single-polarization linear array with/without DG: (a) S11 and S22, (b) S33 and S44, (c) S21, (d) S32, (e) S43, and (f) S42.

The simulated S parameters of the single-polarization linear array with and without DG are given in Fig. 7. Since the array is symmetrical, only the S parameters of Port 1 to Port 4 (see Fig. 2) are shown here. The proposed antenna with DG covers the massive MIMO band of 4.8-5 GHz with -10 dB specification.
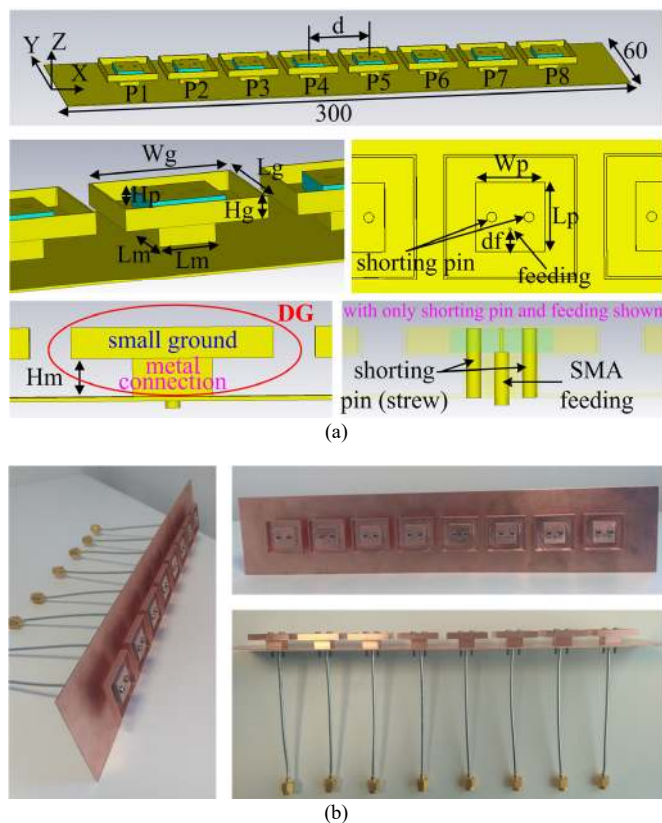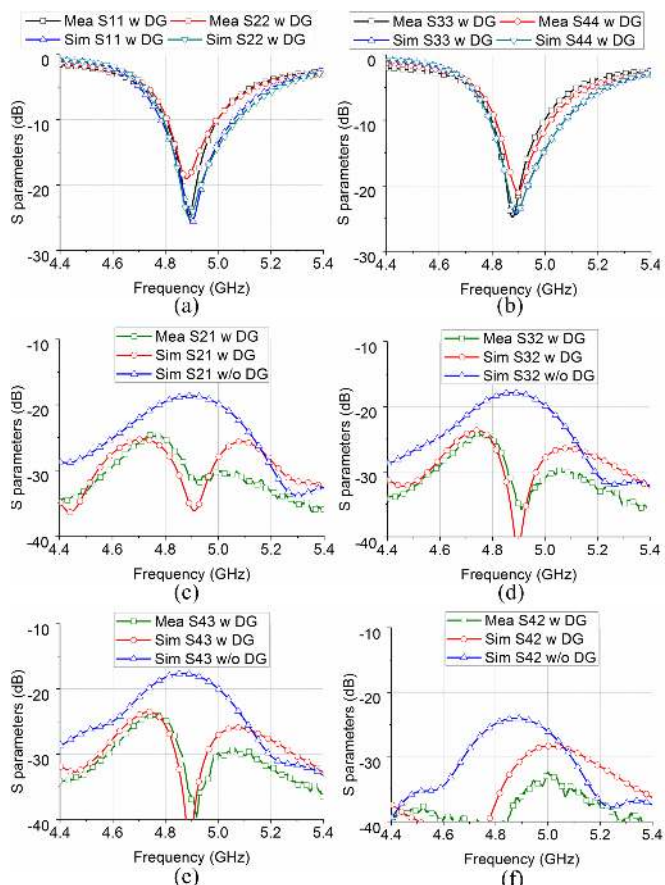

Fig. 6. Single-polarization linear array with 8 elements: (a) the configurations of the antenna array, and (b) the fabricated antenna array with feeding cables.

The bandwidth of the array without DG is about 50 MHz narrower than that with DG, which is not provided in Fig. 7 due to the page length limitation. With the proposed decoupling method, the isolation can be enhanced from 17.5 dB to over 27 dB for all the inter-element coupling within the whole operating band. This method can reduce the mutual coupling not only between the neighboring elements but also between the non-neighboring elements (see Fig. 7 (f)). The S parameters of the antenna prototype are also measured and compared with the simulated in Fig. 7. The measured impedance bandwidth is slightly narrower than the simulated but still covers 4.8-5 GHz. The measured port-to-port isolation is slightly shifted to higher frequencies but still aligns well with the simulated. These small discrepancies are mainly due to the antenna manual fabrication.
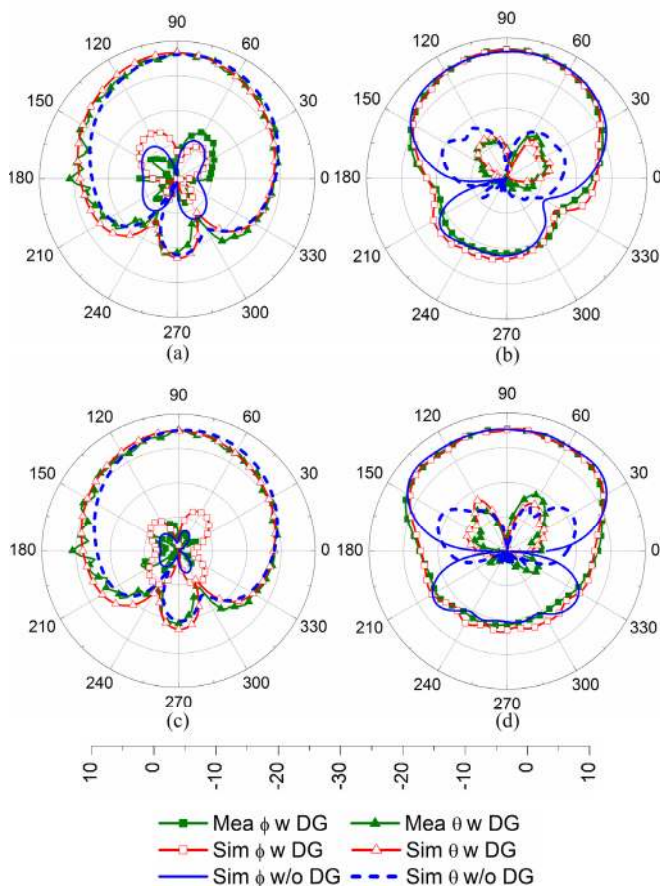

Fig. 8. Simulated and measured radiation patterns of the arrays with/without DG at 4.9 GHz for: (a) E plane (yz plane) of Port 1, (b) H plane (xz plane) of Port 1, (c) E plane (yz plane) of Port 4, and (d) H plane (xz plane) of Port 4.

The simulated and measured radiation patterns of the arrays with/without DG at 4.9 GHz are shown in Fig. 8. The measurements are carried out in a Satimo chamber. During the measurements, when one port is excited, the other ports are terminated with 50-ohm loads. Since the radiation patterns of Port2-Port7 are similar to those of Port4, only the radiation patterns of Port1 and Port4 are depicted here. From the comparison in Fig. 4, it is noticed that: (1) the array with DG has similar radiation patterns in the main lobe direction, lower sidelobe level, and better cross-polarization level compared to the one without DG. This is also one of the advantages of the proposed DG techniques since the decoupling structures should not significantly change or even distort the radiation patterns of a massive MIMO array. (2) The measured and simulated radiation patterns are very similar in both the E plane and H plane.

Fig. 9 shows the simulated and measured total efficiency and realized gain of the arrays with/without DG for all the 8 ports at 4.9 GHz. In the simulations, the total efficiency with DG can be improved by about 6%. The measured total efficiency is slightly lower than the simulated but still over 90% for most of the ports. The realized gain is always over 5 dBi in different cases.

Base on all the comparisons in Fig. 7, Fig. 8 and Fig. 9, it can be concluded that all the measurements agree very well with the simulations. The effectiveness of the proposed DG concept and simulation accuracy have been verified.
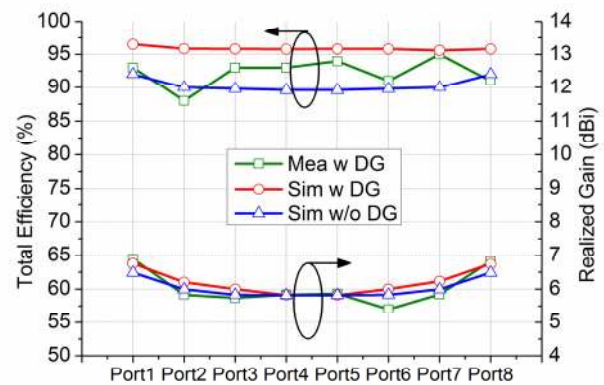

Fig. 9. Simulated and measured total efficiency (left) and realized gain (right) of the arrays with/without DG for all the 8 ports at 4.9 GHz.

In order to show the impact of DG on active VSWR, we follow the same assumptions as that in [21]. That is we assume the 8-element linear array is used as a base station (BS) MIMO array to serve four users simultaneously. Four BPSK data streams are sent to the zero-forcing (ZF) precoder prior to transmission in a Rayleigh fading channel. At one time sample, the BPSK data streams can be denoted as a 4×1 column vector $\mathbf{s}$, the ZF precoder can be expressed as $(\mathbf{H}^H\mathbf{H})^{-1}\mathbf{H}^H$, where $\mathbf{H}$ is a 4×8 MIMO channel matrix and the superscript ^{H} denotes conjugate transpose (or Hermitian). The precoded signal $(\mathbf{H}^H\mathbf{H})^{-1}\mathbf{H}^H\mathbf{s}$ becomes an 8×1 column vector, which is used as weighting coefficients for the 8-element linear array. Since the MIMO channel and the data streams are random, the weighting coefficients are also random. In order to avoid small excitations, the acceptance magnitude threshold of the weighting coefficients is set to 0.2. The largest active reflection coefficient among the eight antenna ports in the frequency range of 4.8-5 GHz is collected for each realization of the random weighting coefficients. Fig. 10 shows the active VSWRs of the 8-element linear array with and without DG. As can be seen, the DG method can effectively reduce the active VSWR.
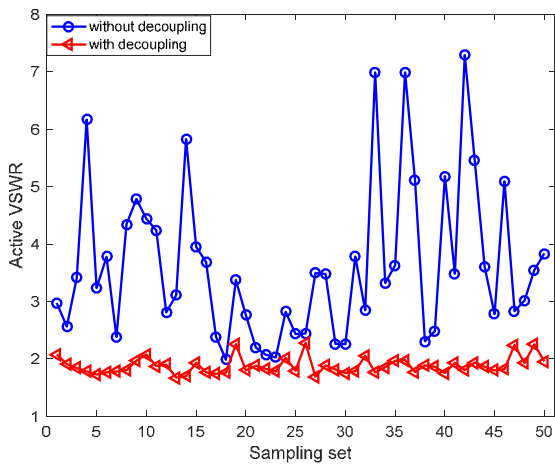
Fig. 10. Comparison of the active VSWR of the 8-element linear arrays with/without DG.

C. Parametric Studies
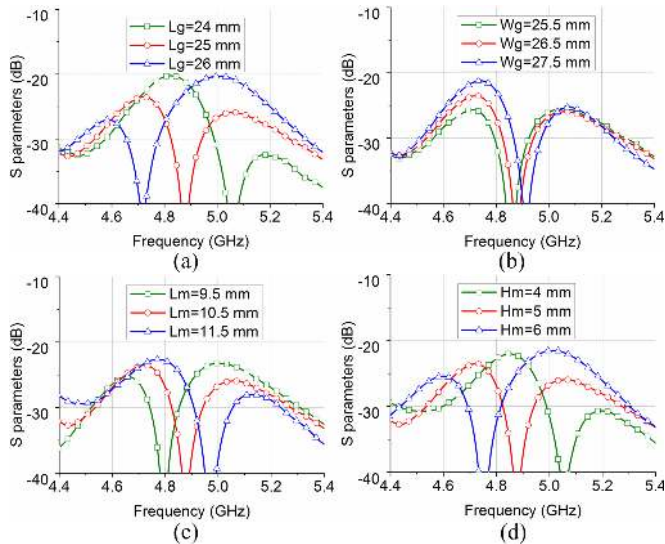

Fig. 11. Parametric studies for (a) Lg, (b) Wg, (c) Lm, and (d) Hm. The parameters of Lg, Wg, Lm, and Hm are defined in Fig. 2.

In order to better understanding the proposed decoupling mechanism, the parameters of *Lg*, *Wg*, *Lm*, and *Hm* (see Fig. 6) have been studied and shown in Fig. 11 (where these parameters have also been mentioned in Section II). Since the mutual coupling of the patch array occurs in the H plane, the path of the coupling currents on the ground plane is much more affected by *Lg*, *Lm*, and *Hm* than *Wg*. As expected, in Fig. 11 the decoupling frequencies move to lower frequencies significantly when increasing the length of *Lg* and *Hm*, and reducing the size of *Lm*. Moreover, *Wg* only slightly varies the frequency with the decoupling property.

IV. DUAL-POLARIZATION SQUARE ARRAY

The accuracy of the simulations has been verified with measurements in Section III. In the following, we will apply the proposed DG technique to enhance the isolation of

dual-polarization 2×2 and 4×4 square arrays with simulations.
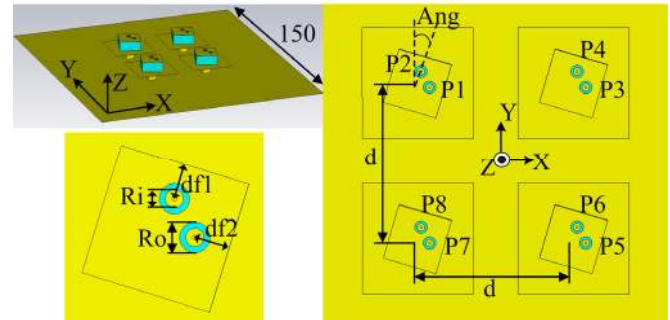
A. Dual-Polarization 2×2 Array

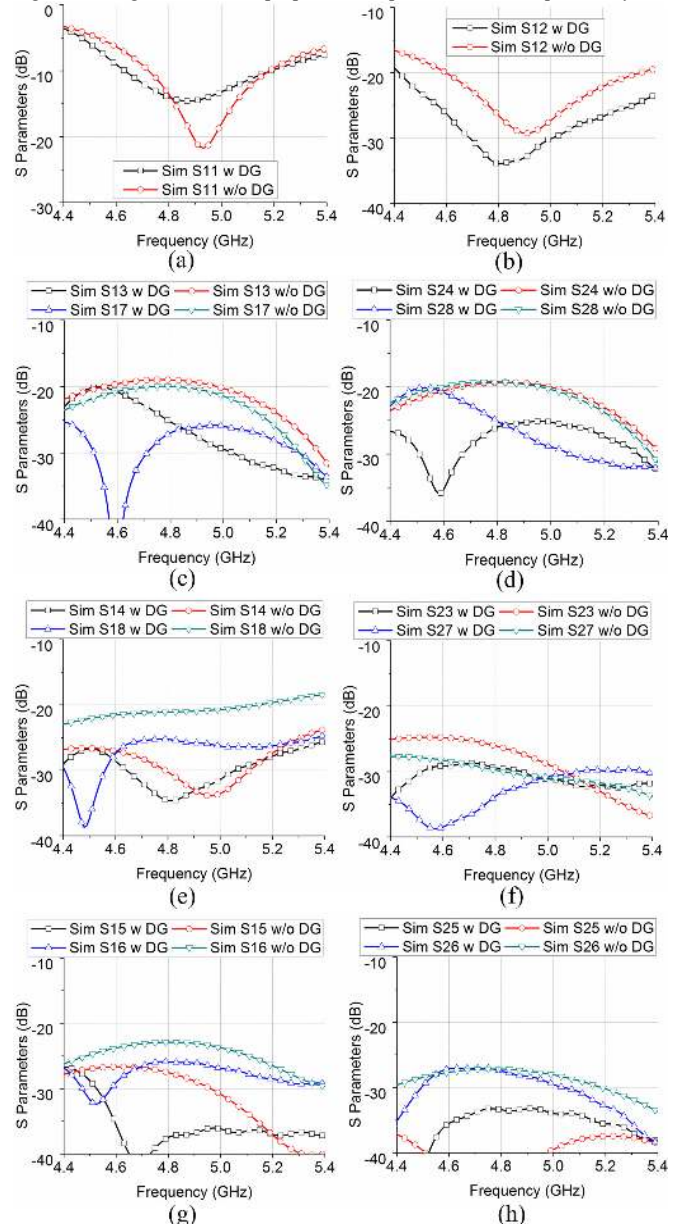Fig. 12. Configurations of the proposed dual-polarization 2×2 square array.

Fig. 13. The simulated S parameters of the dual-polarization 2×2 square array with/without DG: (a) S11, (b) S12, (c) S13 and S17, (d) S24 and S28, (e) S14 and S18, (f) S27 and S23, (g) S15 and S16, and (h) S25 and S26.

Configurations of the proposed dual-polarization 2×2 square array are shown in Fig. 12. The basic dimensions of the array elements and decoupling structures in Fig. 12 are similar to those in Fig. 6. Some geometrical parameters depicted in Fig. 6 can still be used for the array here, which will not be plotted in Fig. 12 again for clarity. The parameters carried over from the previous design are listed as follows: *Wg*, *Lg*, *Hg*, *Lm*, *Hm*, *Lp*, *Wp*, *Hp*, and *df*. The antenna operates at the frequencies of 4.6-5.2 GHz. The array has 4 elements, and each element has two polarizations, where there are 8 ports in total. The inter-element distance *d* is 37 mm (0.57 λ_L). The height of the patch antennas is increased from 3.18 mm in Fig. 6 to 6 mm in Fig. 12 in order to obtain wider bandwidth. The isolation between two ports on each patch highly depends on the feeding positions of *df1* and *df2* (see Fig. 12). Moreover, *df1* and *df2* also significantly vary antenna impedance matching. Therefore, two ring slits have been etched on the patch to form the capacitive feeding [25], where good impedance matching can always be obtained with the given feeding positions of *df1* and *df2*. In addition, each patch element has also been rotated by an angle of *Ang* = 16º. The detailed antenna dimensions are also given in Table I. The total array height (including the DG) in this design is 0.199 λ_L, which is still lower than the linear array height of 0.275 λ_L with ADS in [21].

Since the geometry of a dual-polarization 2×2 square array is symmetrical, the shapes of the small ground plane and the metal cylinder cross-section have to be square in order to achieve the high overall isolation between all the 8 ports. However, for each polarization, the mutual coupling between two patch elements placed along the E plane and H plane is not the same. It means that with a square-shaped DG, the decoupling of the patch elements in E plane and H plane will typically not occur at the same frequency. The dimensions of DG are optimized in order to make a trade-off between the E-plane and H-plane decoupling. The simulated S parameters of the dual-polarization 2×2 square array with/without DG are depicted in Fig. 13. The proposed 2×2 array works at the frequencies of 4.8-5.2 GHz. For all the co- and cross-polarization coupling, only S25 distorts from below -40 dB to about -35 dB, which is still kept at a very low level. The isolation of all the other coupling can still be improved efficiently, although the decoupling of different elements and polarization may not happen simultaneously at the central frequency. In other words, the decoupling out of the resonant decoupling frequency is still efficient, so this method gives a relatively wide decoupling bandwidth. In addition, the rotation angle of *Ang* = 16º makes a trade-off between the coupling of different elements and polarizations, which further improves the worst isolation from all the ports by around 1 dB. With the DG, the coupling in the band of 4.8-5.2 GHz has been suppressed to be below -25.1 dB for all the coupling. The isolation here is much lower than that in [18]. Additionally, it should be noticed that due to the slightly different decoupling resonant frequencies of the port 1 with all the other ports, the decoupling is still a dual-element model (shown in Section II). Indeed, there may be some contributions from the elements out of this dual-element model system, but the contributions are not very significant.
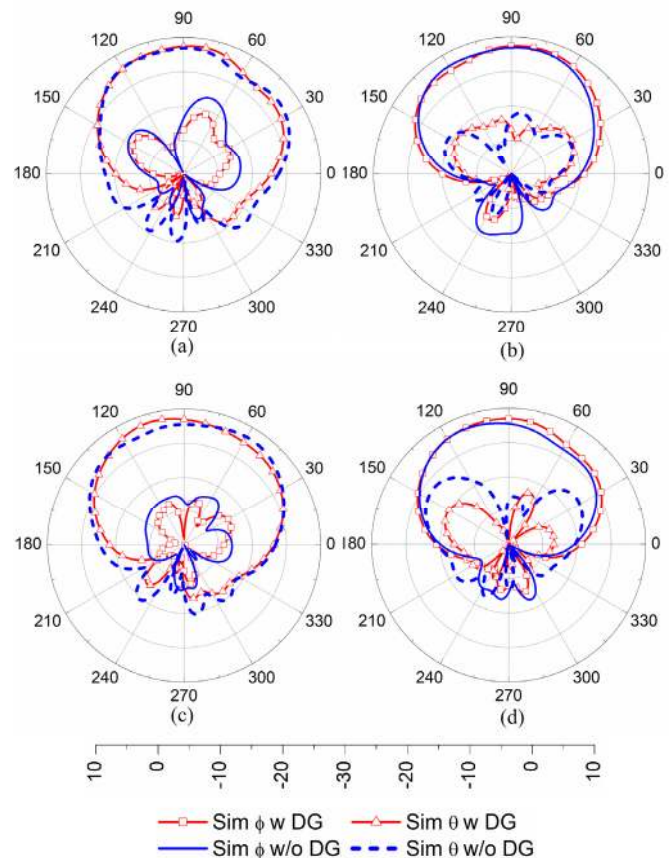

Fig. 14. Simulated radiation patterns of the arrays with/without DG at 4.9 GHz for: (a) E plane of Port 1, (b) H plane of Port 1, (c) E plane of Port 2, and (d) H plane of Port 2. Please note that the E plane of Port 1 and the H plane of Port 2 are in the same plane of phi=90º- *Ang*=74º, while the H plane of Port 1 and the E plane of Port 2 are in the same plane of phi=180º- *Ang*=164º. (*Ang*=16 º)

The radiation patterns of the arrays with/without DG at 4.9 GHz are simulated and plotted in Fig. 14. The conclusions are similar to those of the linear array in Section III: the radiation patterns in the main lobe direction are nearly the same with and without DG. Moreover, the side lobe and cross-polarization of the radiation patterns are improved after adding the DG. The simulated total efficiency of the arrays with and without DG is always higher than 91%. The realized gain of the array with the DG is over 7.3 dBi, while the one without DG is 6.8 dBi.

The active VSWR of the dual-polarization 2×2 square array with/without DG has also been calculated and drawn in Fig. 15 with the same setups to those in the linear array in Section III. By suppressing the mutual coupling with DG, the active VSWR is below 2 in almost all the different excitation scenarios. In addition, the 0º or 16º in Fig. 15 means the *Ang* = 0º or 16º (see Fig. 12). Without DG, the active VSWR of antenna elements rotated and not rotated by 16º is also compared in Fig. 15. The active VSWR in these two cases is more or less the same on average, which prove that rotation without DG does not improve the active VSWR and the DG is the main reason for the active VSWR improvement
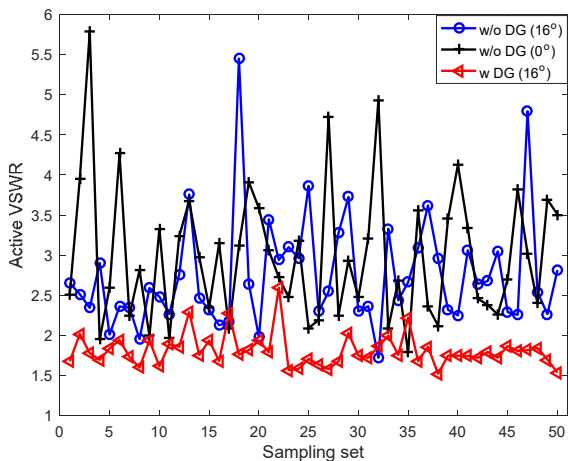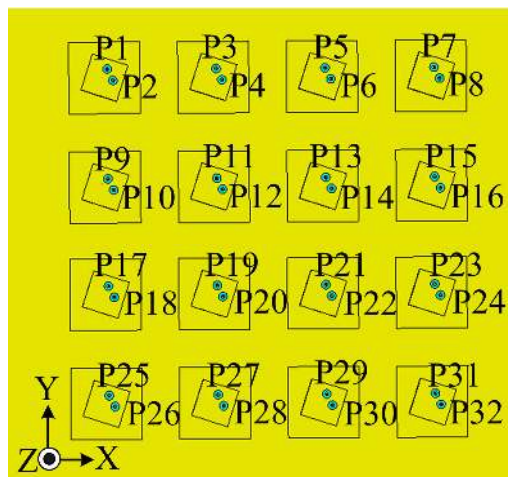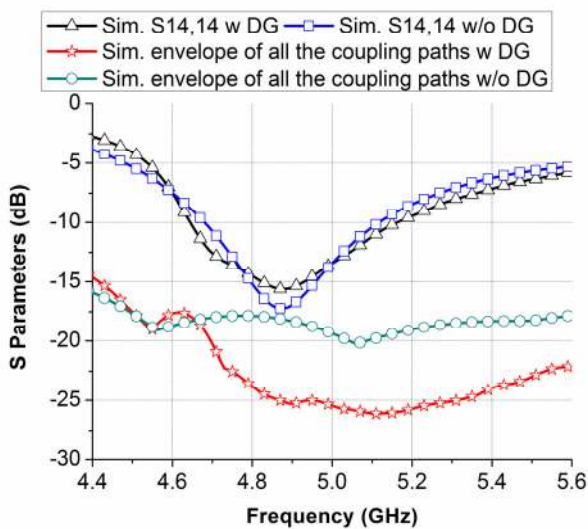
Fig. 15. Comparison of the active VSWR of the dual-polarization 2×2 square array with/without DG.

B. Dual-polarization 4×4 Array

(a)

(b)

Fig. 16. Dual-polarization 4×4 square array: (a) the configurations, and (b) the S parameters of Element 14 with/without DG.

If the proposed decoupling method can also be used in a 4×4 square array, it means the proposed DG technique can enhance the isolation of the square array with any element number. Therefore, the 2×2 array in Section IV-A has been modified into a dual-polarization 4×4 square array with the same inter-element space. The configurations of the 4×4 array are illustrated in Fig. 16 (a), where there are 16 elements with 32 ports in total. The detailed dimensions can be found in Table I as well. The S parameters of the Port14 are plotted in Fig. 16 (b). There are mainly two reasons to only show the results of Port14: (1) Port14 is fully embedded in the other elements, which is the worst scenario for decoupling; (2) Port14 has slightly stronger mutual coupling than Port13. In addition, the curves with the mutual coupling lower than -28 dB are not added in Fig. 16 (b) for clarity. It can be observed that the isolation is efficiently enhanced with DG especially within the band of 4.8-5.2 GHz. In 4.8-5.2 GHz, the improvement of about 7 dB isolation (from 17.8 dB to 24.5 dB) has been obtained for all the ports.

V. PERFORMANCE COMPARISON

TABLE II
PERFORMANCE COMPARISON

Ref.	Array Config.	Pol.	Band (GHz)	Worst Isolatoin (dB)	Height (λ_C)	Largest Distance (λ_C)
[20]	1×7	Single	26.6-30	27	5	-------
[21]	1×8	Single	2.4-2.5	24	0.31	0.45
	2×2	Dual	3.3-3.8	20	0.30	0.71
[18]	4×4 or larger	Dual	4.9-6	14	0.24	0.55
This work	1×8	Single	4.8-5	27	0.14	0.52
	2×2	Dual	4.8-5.2	25.1	0.22	0.62
	4×4 or larger	Dual	4.8-5.2	24.5	0.25	0.62

The performance of the proposed arrays with DG has been compared with the recently reported literature. The height in [20] is much higher than the proposed 1×8 array with similar isolation. The profile and isolation of the proposed 1×8 and 2×2 arrays is much lower and higher than the ones in [21], respectively. The inter-element distances in this paper are slightly larger but still comparable to those in [21]. In addition, though [20] and [21] have mentioned their techniques can be used for massive MIMO, no results of a large array (e.g., a 4×4 array) have been given. [18] has proposed a large array, but the mutual coupling is over 10 dB higher than that in this paper with the other figures of merits comparable

VI. CONCLUSIONS

In this paper, the concept of the DG has been introduced and the operating principle has been explained. A single-polarization linear array with DG has been proposed, fabricated and measured. Measurements agree well with the simulations, which has verified the concept and the simulation accuracy. Another two examples of dual-polarization square arrays have also been designed and simulated. In all of these cases, the isolation has been enhanced efficiently with the proposed decoupling technique of DG. Compared with the previous work, the arrays in this paper realize much better isolation with a low profile than the one in [18] and achieve much lower profile with comparable isolation than the ones in [19]-[21].

REFERENCES

[1] R. G. Vaughan and J. B. Andersen, "Antenna diversity in mobile communications", *IEEE Trans. Vehic. Technol.* vol. 36, no. 4, pp. 149-172, Nov. 1987.

[2] R. He, B. Ai, G. L. Stuber, *et al.*, "Geometrical based modeling for millimeter wave MIMO mobile-to-mobile channels," *IEEE Trans. Veh. Technol.*, vol. 67, no. 4, pp. 2828-2863, Apr. 2018.

[3] Y. Xin, D. Wang, J. Li, *et al.*, "Area Spectral Efficiency and Area Energy Efficiency of Massive MIMO Cellular Systems," *IEEE Trans. Veh. Technol.*, vol. 65, no. 5, pp. 3243-3254, May 2016.

[4] E. G. Larsson, O. Edfors, F. Tufvesson, and T. L. Marzetta, "Massive MIMO for Next Generation Wireless Systems," *IEEE Communications Magazine*, vol. 52, pp. 186-195. Feb 2014.

[5] D. A. Basnayaka, M. D. Renzo, and H. Haas, "Massive but few active MIMO," *IEEE Trans. Veh. Technol.*, vol. 65, no. 9, pp. 6861-6877, 2016.

[6] P. Pan, H. Wang, Z. Zhao, and W. Zhang, "How many antenna arrays are dense enough in massive MIMO systems," *IEEE Trans. Veh. Technol.*, vol. 67, no. 4, pp. 3042-3053, 2018.

[7] X. Chen, S. Zhang, and Q. Li, "A review of mutual coupling in MIMO systems." *IEEE Access*, vol. 6, pp. 24706-24719, 2018.

[8] D. M. Pozar, "A relation between the active input impedance and the active element pattern of a phased array," *IEEE Trans. Antennas Propag.*, vol. 51, no. 9, pp. 2486–2489, Sep. 2003.

[9] C. Fager, X. Bland, K. Hausmair, et al. "Prediction of smart antenna transmitter characteristics using a new behavioral modeling approach," *IEEE MTT-S Int. Microw. Symp.*, Tampa, FL, Jun. 1-6, 2014, pp. 1-4.

[10] C.-Y. Chiu, C.-H. Cheng, R. D. Murch, and C. R. Rowell, "Reduction of mutual coupling between closely-packed antenna elements," *IEEE Trans. Antennas Propag*, vol. 55, no. 6, pp. 1732–1738, Jun. 2007.

[11] B. K. Lau and J. B. Andersen, "Simple and efficient decoupling of compact arrays with parasitic scatterers," *IEEE Trans. Antennas Propagat.*, vol. 60, no. 2, pp. 464–472, Feb. 2012

[12] S. Zhang and G. F. Pedersen, "Mutual coupling reduction for UWB MIMO antennas with a wideband neutralization line," *IEEE Antennas Wireless Propag. Lett.*, vol. 15, pp. 166-169, 2016.

[13] J. C. Coetzee and Y. Yu, "Port decoupling for small arrays by means of an eigenmode feed network," *IEEE Trans. Antennas Propag.*, vol. 56, no. 6, pp. 1587-1593, Jun. 2008.

[14] G. Zhai, Z. N. Chen, and X. Qing, "Enhanced isolation of a closely spaced four-element MIMO antenna system using metamaterial mushroom," *IEEE Trans. Antennas Propag.*, vol. 63, no. 8, pp. 3362–3370, Aug. 2015.

[15] L. Y. Zhao and K. L. Wu, "A decoupling technique for four-element symmetric arrays with reactively loaded dummy elements," *IEEE Trans. Antennas Propag.*, vol. 62, no. 8, pp. 4416–4421, Aug. 2014.

[16] W. Su, Q. Zhang, S. Alkaraki, Y. Zhang, X.-Y. Zhang, and Y. Gao, "Radiation energy and mutual coupling evaluation for multimode MIMO antenna based on the theory of characteristic mode," *IEEE Trans. Antennas Propag.*, vol. 67, no. 1, pp. 74–84, Jan. 2019.

[17] S. Saber, and R. D. Murch, "A compact planar printed MIMO antenna design," *IEEE Trans. Antennas Propag.*, vol. 63, no. 3, pp. 1140-1149, Mar. 2015.

[18] M. V. Komandla, G. Mishra, and S. K. Sharma. "Investigations on dual slant polarized cavity-backed massive MIMO antenna panel with beamforming," *IEEE Trans. Antennas Propag.*, vol. 65, no. 12, pp. 6794-6799, Dec. 2017.

[19] Y. Gao, R. Ma, Y. Wang, Q. Zhang, and C. Parini. "Stacked patch antenna with dual-polarization and low mutual coupling for massive MIMO," *IEEE Trans. Antennas Propag.*, vol. 64, no. 10, pp. 4544-4549., Oct. 2016.

[20] M. Jiang, Z. N. Chen, Y. Zhang, W. Hong, and X. Xuan, "Metamaterial-based thin planar lens antenna for spatial beamforming and multibeam massive MIMO," *IEEE Trans. Antennas Propag.*, vol. 65, no. 2, pp. 464-472, Feb. 2017.

[21] K.-L. Wu, C. Wei, X. Mei, and Z. Zhang, "Array-antenna decoupling surface," *IEEE Trans. Antennas Propag.*, vol. 65, no. 12, pp. 6728-6738, Dec. 2017.

[22] Y. Gao, X. Chen, Z. Ying and C. G. Parini, "Design and performance investigation of a dual-element PIFA array at 2.5 GHz for MIMO terminal," *IEEE Trans. Antennas Propag.*, vol. 55, no. 12, pp. 3433 - 3441, Dec. 2007.

[23] B. Xu, K. Zhao, Z. Ying, S. He and J. Hu, "Investigation of surface waves suppression on 5G handset devices at 15 GHz," *the 10th European Conf. Antennas Propag. (EuCAP)*, 10-15 Apr., 2016.

[24] K. Zhao, S. Zhang, and S. He, "Closely-located MIMO antennas of triband for WLAN mobile terminal applications," *Journal of Electromagnetic Waves and Applications*, vol. 24, 363-371, 2010.

[25] P. S. Hall, "Probe compensation in thick microstrip patches," *Electron. Lett.*, vol. 23, pp. 606–607, 1987.